

2019

Quantifying the Concentration and Penetration Depth of Long-Lived RONS in Plasma Activated Water by UV Absorption Spectroscopy

Zhijie Liu

Chunxi Zhou


Dingxin Liu

Tongtong He

Li Guo

See next page for additional authors

Follow this and additional works at: https://digitalcommons.odu.edu/bioelectrics_pubs

 Part of the [Biomedical Commons](#), and the [Engineering Physics Commons](#)

Repository Citation

Liu, Zhijie; Zhou, Chunxi; Liu, Dingxin; He, Tongtong; Guo, Li; Xu, Dehui; and Kong, Michael G., "Quantifying the Concentration and Penetration Depth of Long-Lived RONS in Plasma Activated Water by UV Absorption Spectroscopy" (2019). *Bioelectrics Publications*. 268.

https://digitalcommons.odu.edu/bioelectrics_pubs/268

Original Publication Citation

Liu, Z. J., Zhou, C. X., Liu, D. X., He, T. T., Guo, L., Xu, D. H., & Kong, M. G. (2019). Quantifying the concentration and penetration depth of long-lived RONS in plasma-activated water by UV absorption spectroscopy. *AIP Advances*, 9, (015014) 015011-015012.

doi:10.1063/1.5037660

Authors

Zhijie Liu, Chunxi Zhou, Dingxin Liu, Tongtong He, Li Guo, Dehui Xu, and Michael G. Kong

Quantifying the concentration and penetration depth of long-lived RONS in plasma-activated water by UV absorption spectroscopy

Cite as: AIP Advances 9, 015014 (2019); doi: 10.1063/1.5037660

Submitted: 26 April 2018 • Accepted: 3 January 2019 •

Published Online: 14 January 2019



View Online



Export Citation



CrossMark

Zhijie Liu,^{1,a)} Chunxi Zhou,¹ Dingxin Liu,¹  Tongtong He,¹ Li Guo,¹ Dehui Xu,¹ and Michael G. Kong^{1,2,3,a)}

AFFILIATIONS

¹State Key Laboratory of Electrical Insulation and Power Equipment, Centre for Plasma Biomedicine, School of Electrical Engineering, Xi'an Jiaotong University, Xi'an, Shaanxi 710049, PR China

²Frank Reidy Center for Bioelectrics, Old Dominion University, Norfolk, Virginia 23508, USA

³Department of Electrical and Computer Engineering, Old Dominion University, Norfolk, Virginia 23529, USA

^{a)}Correspondence should be addressed to Z.J. Liu (Email: liuzhijie2010@163.com) and M.G. Kong (Email: mglin5g@gmail.com)

ABSTRACT

Reactive oxygen and reactive nitrogen species (RONS) are believed to play a key role in biomedical applications, which means that RONS must reach the target tissue to produce a therapeutic effect. Existing methods (electron spin spectrometry and microplate reading) to determine the RONS concentration are not suitable for experimental real-time measurements because they require adding an indicating reagent to the plasma-treated medium, which may alter the chemical composition of the medium. In this paper, we propose a method to measure the long-lived RONS concentration in plasma-activated water (PAW) by using UV absorption spectroscopy. Based on an analysis and fit of the absorption spectra of standard solutions (H_2O_2 , NaNO_2 , and NaNO_3), we propose a detailed fitting procedure that allows us to calculate the concentrations of simplex H_2O_2 , NO_2^- , and NO_3^- . The results show that the pH and the cross reactivity between RONS in PAW correlate strongly with the absorption spectra. To confirm the accuracy of the calculations, we also use a microplate reader and add chemical reagents to measure the concentrations of H_2O_2 , NO_2^- , and NO_3^- . The results show that the concentrations calculated by the proposed fitting method are relatively accurate and that the error range is acceptable. Additionally, the time-dependent diffusion of RONS in PAW is measured and analyzed at different depths in the PAW. This fitting approach constitutes a noninvasive approach to measure RONS at different depths in PAW.

© 2019 Author(s). All article content, except where otherwise noted, is licensed under a Creative Commons Attribution (CC BY) license (<http://creativecommons.org/licenses/by/4.0/>). <https://doi.org/10.1063/1.5037660>

I. INTRODUCTION

Reactive oxygen and reactive nitrogen species (RONS) such as OH , O_2^- , H_2O_2 , NO_2^- , NO_3^- , ONOO^- , etc. are generated by non-thermal plasmas at atmospheric pressures and are believed to play a key role in biomedical applications, such as disinfection, wound healing, and cancer therapy.¹⁻³ Generally, the use of plasma to treat tissue in the context of plasma medicine often involves a thin intervening liquid layer on top of the tissue.⁴⁻⁶ The RONS produced in the gas phase first solvate into the liquid and then react in the liquid layer prior to reaching the tissue,⁶⁻⁸ sometimes even generating

secondary RONS within the liquid before reaching the surface of the underlying tissue.⁸⁻¹⁰ Although numerous works have studied how RONS affect plasma-activated water (PAW) when cell inactivation is induced,^{4-8,11-20} the actual physical mechanism of the inactivation remains unclear, and one of the most important reasons for this situation is that precisely determining the constituents and production of RONS in solution form a critical bottleneck because of the lack of effective technical methods to measure the spatial and temporal RONS distribution.²¹⁻²⁴

Existing methods (microplate reader and electron spin resonance spectrometry) to determine the concentration of

RONS in the liquid phase have certain limitations: First, they only detect a single species in the liquid. Second, they cannot measure the time-dependent RONS concentration in solution. Third, they require the addition of specific chemical reagents (such as chromogenic agent, capture agent, scavengers, etc.) to the solution,^{25,26} which may destroy the chemical pathways and the balance of reaction dynamics and thereby modify the composition of the original solution. In addition, the selectivity of these methods has to be considered because some scavengers interact with several species.²⁶ Therefore, to overcome the disadvantages of existing techniques, other methods are required to quantitatively determine the concentration of RONS in PAW without using chemical reagents.^{21,24}

Ultraviolet (UV) absorption spectroscopy is a simple and convenient method to detect the concentration of RONS in PAW.^{23,24,27-31} UV absorbance reveals the presence of RONS and the magnitude of UV absorption gives the RONS concentration.²⁷ In general, the RONS concentration in liquid is measured by using UV-visible spectroscopy combined with chemical probes. For example, Baeketal *et al.* measured the density of OH radicals in plasma-treated liquids by using UV absorption spectroscopy and the hydroxylation of terephthalic acid, which is a typical photocatalytic reaction that specifically oxidizes terephthalic acid (i.e., the OH radical reacts with terephthalic acid to form hydroxyl terephthalic acid, which fluoresces).²³ He *et al.* measured the concentration of H₂O₂, NO₂⁻, and NO₃⁻ in PAW by using UV absorption spectroscopy with chemical reagents (Amplex[®] Red reagent, Anitrate Reductase Enzyme, and Griess Reagent).³¹ Oh *et al.* used UV-Vis spectroscopy to monitor RONS transport in PAW without using chemical probes, and they developed a fitting procedure to obtain the absorption lines of H₂O₂, NO₂⁻, and NO₃⁻ from the total absorbance of RONS.^{24,27,28} An automated program fits the UV spectra to more rapidly process larger datasets and to accurately measure the concentrations of H₂O₂, NO₂⁻, and NO₃⁻ in PAW, which allows the concentration of long-lived aqueous reactive species to be measured. However, how the pH and the cross reactivity in PAW affect the absorption has yet to be addressed, which motivates us to propose an optimized method based on UV spectroscopy to quantify the production and penetration depth of long-lived RONS in PAW. This work thus considers how the pH and cross reactivity affect the UV absorption and proposes a fitting method based on UV absorption that gives the concentration of H₂O₂, NO₂⁻, and NO₃⁻ in PAW. The time-dependent diffusion of RONS in PAW is also measured and analyzed.

II. EXPERIMENTAL METHODS

A. UV absorption spectroscopy

A conventional double-beam UV-Vis spectrophotometer (Shimadzu U-1800) was used to detect the absorption spectra of RONS in PAW. The samples were contained in a quartz cuvette (100-QS, Hellma Analytics) and had a standard optical path of 10 mm. The instrumental accuracy was 0.001, and

the transmission spectra were recorded from 190 to 900 nm. Oh *et al.*^{27,28} confirmed that the absorption spectra of RONS extends below 300 nm (into the UV) and that no absorption occurs in the visible and near infrared (400–900 nm). The spectral resolution was 0.2 nm and the scan speed was 120 nm/min. The RONS concentration was determined from absorbance (Abs) spectra by using the Beer-Lambert law^{23,28,30}

$$\text{Abs}(\lambda) = \varepsilon lc, \quad (1)$$

where ε is the molar absorptivity of the chemical species at a certain wavelength λ , l is the optical path length, and c is the RONS concentration. However, the use of Eq. (1) would lead to large errors in the calculated concentration of H₂O₂, NO₂⁻, and NO₃⁻ because the absorption lines of H₂O₂, NO₂⁻, and NO₃⁻ overlap each other between 190 and 230 nm.^{27,28} We therefore separate the total absorbance of RONS to obtain the single absorption lines of H₂O₂, NO₂⁻, and NO₃⁻, following which we calculate the corresponding concentration by using Eq. (1). In this way, the calculated value is more accurate than what can be obtained by using only the total absorption lines.

B. Measuring RONS concentrations

The present experiments were all done at 25 °C because the absorption spectra are sensitive to the ambient temperature. Standard solutions of H₂O₂, NaNO₂, and NaNO₃ were diluted to different concentrations and used to measure the absorbance. A surface dielectric barrier discharge system was used to generate a surface plasma in air, and deionized water in a petri dish was placed underneath the surface plasma to confirm the accuracy of the RONS concentration in PAW as detected by UV-Vis spectroscopy. In addition, the concentration of H₂O₂, NO₂⁻, and NO₃⁻ was also measured by using a microplate reader (Thermo Scientific Varioskan[®] Flash Reader) and adding chemical reagents.

To measure H₂O₂, Amplex[®] Red reagent was added to the PAW to react with H₂O₂ in a 1:1 stoichiometry and produce the red-fluorescent oxidation product. This product may be excited at $\lambda = 550$ nm and emits at $\lambda = 595$ nm. To detect NO₂⁻, the Griess reagent was added to the PAW, and the absorbance was measured at $\lambda = 540$ nm. Next, the nitrate reductase enzyme and Griess reagent were added to the PAW to measure the concentrations of nitrate and nitrite at the same wavelength. Finally, the NO₃⁻ concentration was obtained by subtracting the NO₂⁻ concentration from the total concentration of NO₂⁻ and NO₃⁻ (a similar method is discussed in our previous work^{7,26,31}).

III. RESULTS AND DISCUSSION

A. UV absorption spectra of RONS

According to Ref. 28, long-lived RONS (H₂O₂, NO₂⁻, and NO₃⁻) are the main species contributing to the UV absorbance between 190 and 340 nm. To confirm this result, the absorption lines of H₂O₂, NO₂⁻, and NO₃⁻ were obtained from the

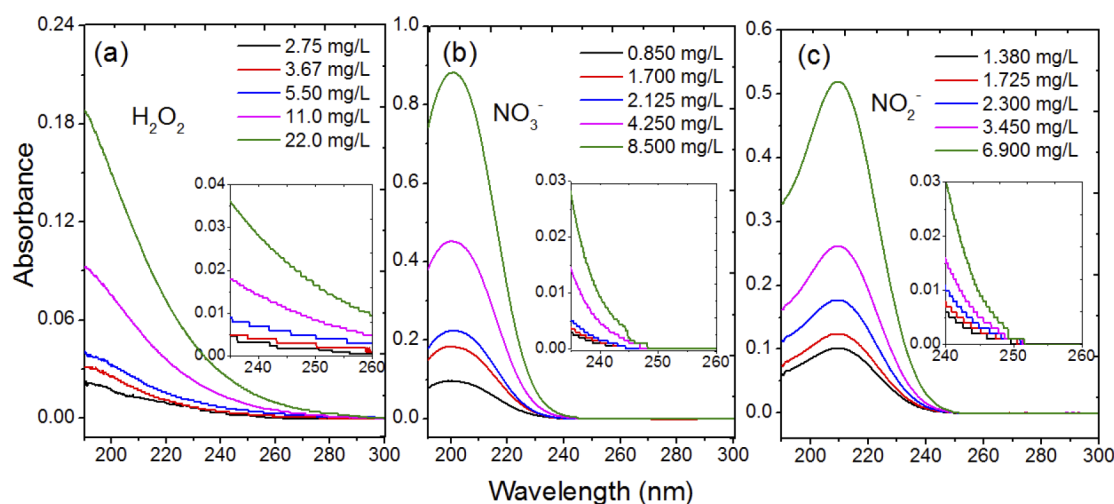


FIG. 1. UV absorption spectra of (a) H_2O_2 , (b) NO_2^- , and (c) NO_3^- for various concentrations of standard solution.

standard solutions for H_2O_2 , NaNO_2 , and NaNO_3 , respectively, under different concentrations. The resultant UV absorption spectra are shown in Figs. 1(a)–1(c), respectively. Figure 1 gives the following results: First, each standard solution has its specific maximum-absorption wavelength: that for H_2O_2 may be below 190 nm, that for NaNO_3 is at about 203 nm, and that for NaNO_2 is at about 210 nm. Second, the absorbance at the given wavelength increases with increasing concentration of the standard solution, and the absorbance of H_2O_2 , NO_2^- , and NO_3^- is almost linear in the concentration of standard solution, which is consistent with the experimental results reported in Ref. 32. Third, H_2O_2 may contribute to the broad spectra from 190 to 280 nm in Fig. 1, whereas NO_2^- and NO_3^- contribute only to the broad peak at 190–250 nm, so only H_2O_2 contributes to the absorbance from 250 to 280 nm. This is very important because the absorbance in the range 250–280 nm helps us to establish a quantitative relationship between absorbance and H_2O_2 concentration and thereby to determine the concentration of H_2O_2 in mixed RONS in PAW.

However, the spectra of standard solutions in Fig. 1 have different y-axis scales and use different standard concentrations of the relevant species, which may lead to confusion about the actual contributions to the overall spectrum. Therefore, the insets show expanded views from 235 to 260 nm. Note that the contributions of NO_2^- and NO_3^- are prominent above 250 nm when the concentrations of NO_2^- and NO_3^- exceed about 0.5 and 1 mM, respectively. Thus, in these experiments, we focus only on low concentrations of RONS (less than 0.5 mM), because, in plasma biomedical applications, organisms (such as myeloma cancer cells) would be killed when exposed to tens of μM of RONS. Moreover, during the plasma-liquid interactions, the concentrations of H_2O_2 , NO_2^- , and NO_3^- beyond the mM level are quantified from the first derivative of the absorption spectra.³³

B. Dependence of pH and hybrid species on RONS profiles

A solution exposed to a plasma jet or surface-discharge plasma becomes acidic, with a pH that depends on the treatment time. The formation of H^+ may strongly affect the rates of generation and consumption of aqueous reactive species,^{2,34,35} such as OH , NO_2^- , and ONOO^- . In other words, it may affect the absorbance spectra. In this section, we study how pH affects the absorption lines by measuring standard solutions of H_2O_2 , NaNO_2 , and NaNO_3 . The absorption spectra of H_2O_2 , NO_2^- , and NO_3^- are shown in Fig. 2 for pH from 4 to 7. The influence of pH on the absorption spectra of H_2O_2 and NO_2^- varies, but pH does not affect the absorption spectra of NO_3^- . For NO_2^- , the pH mainly influences the characteristic peak. Above 220 nm (in the tail of the absorption), the pH has no effect on the absorption spectra for NO_2^- and NO_3^- . However, the opposite is true for H_2O_2 . These results allow us to develop a fitting procedure to determine the concentrations of H_2O_2 , NO_2^- , and NO_3^- .

In PAW, a variety of species may mix and react with each other to generate acidic conditions. For instance, H_2O_2 can react with NO_2^- to form NO_3^- to a certain extent due to the oxidation of H_2O_2 and the presence of H^+ .^{36–38} Therefore, to study how mixing the solutions affects the absorption spectra, we mixed H_2O_2 with NaNO_2 , H_2O_2 with NaNO_3 , and NaNO_2 with NaNO_3 and measured their absorption spectra. Figure 3 shows the spectra of the mixed solutions with the fitted spectra superposed for the absorbance of the two-type single reactive species shown in Fig. 1. The results show that the measured spectra between 200 and 220 nm fall slightly below the fitted spectra for the $\text{H}_2\text{O}_2+\text{NaNO}_3$ and $\text{NaNO}_3+\text{NaNO}_2$ mixed solutions. A larger discrepancy occurs between the measured result and the fit from 200 to 220 nm for the $\text{H}_2\text{O}_2+\text{NaNO}_2$ mixed solution, which may be attributed to the cross reactivity between H_2O_2 and NaNO_2 that occurs in the

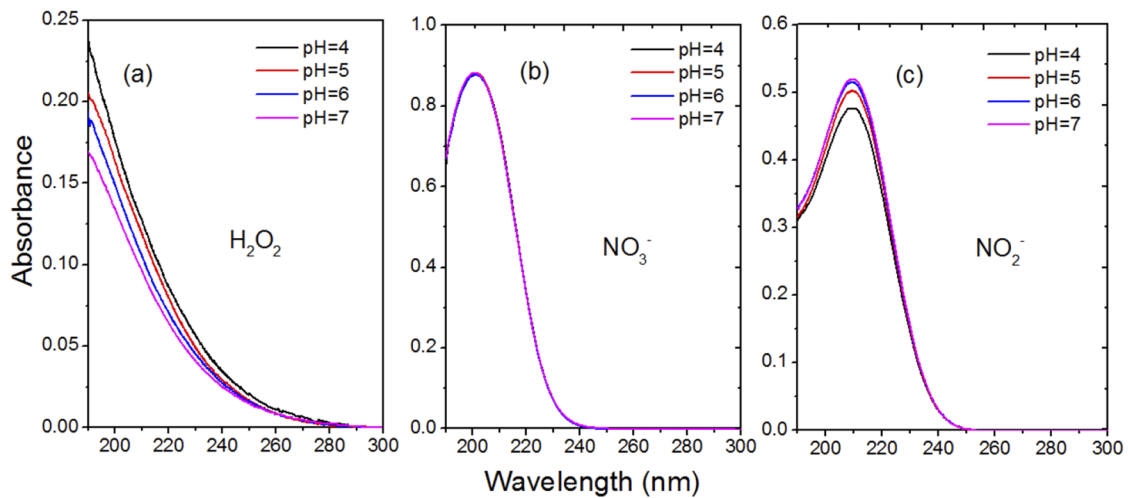


FIG. 2. UV absorption spectra of H_2O_2 , NO_2^- , and NO_3^- for various pH.

solution and that reduces the measured result.^{39,40} However, the measured spectra are very close to the fitted spectra from 220 to 250 nm for the three mixed solutions. Another important phenomenon is that the absorbance in Fig. 3(c) goes to zero above 250 nm, whereas the absorbance remains nonzero at 250 nm in Figs. 3(a) and 3(b) and only goes to zero at 260 or 270 nm. This result fully illustrates that only H_2O_2 contributes to the absorbance above 250 nm.

In addition, $\text{H}_2\text{O}_2+\text{NaNO}_2+\text{NaNO}_3$ mixed solutions were also prepared with different concentrations, and their absorption spectra are shown in Fig. 4. Evidence of the cross reactions in the mixed solutions appears between 200 and 220 nm, which slightly shifts the absorption peak and changes the

shape of the absorption band. However, this change has only a small effect on the absorption peak and little effect on the tail. Therefore, to reduce the impact and improve the accuracy of the results, we use the spectral tail to analyze and calculate the RONS concentration. Furthermore, the spectra in Fig. 4 are consistent with the spectra in PAW obtained by spectrophotometer (see Fig. 8), which also confirms that H_2O_2 , NO_2^- , and NO_3^- are the main species contributing to the absorbance between 190 and 300 nm.

C. Absolute concentration of H_2O_2 in PAW

An urgent and crucial question is how to calculate the concentrations of H_2O_2 , NO_2^- , and NO_3^- in PAW by using

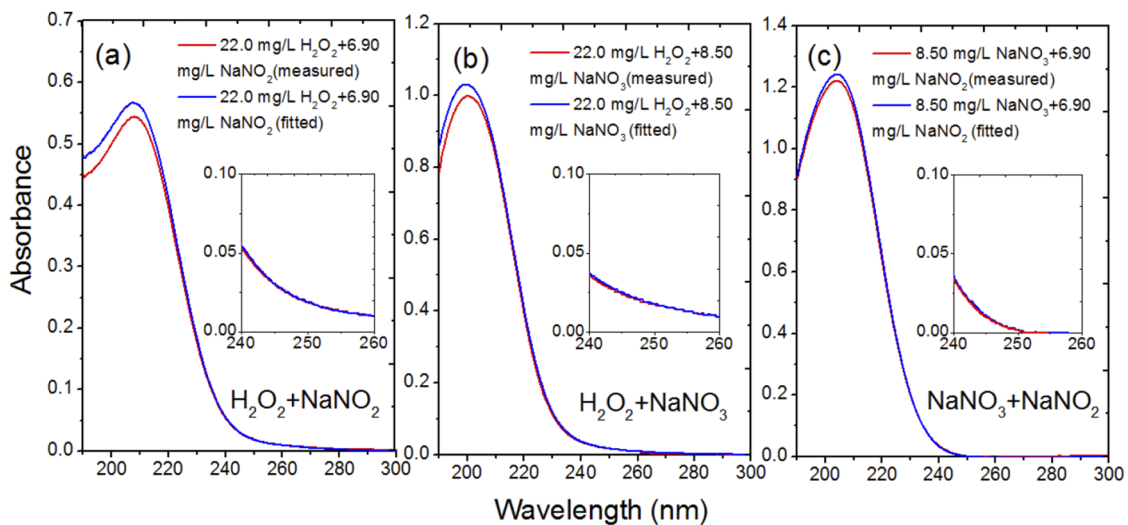


FIG. 3. Absorption spectrum of (a) $\text{H}_2\text{O}_2+\text{NaNO}_2$ solution, (b) $\text{H}_2\text{O}_2+\text{NaNO}_3$ solution, and (c) $\text{NaNO}_2+\text{NaNO}_3$ solution. The measured spectra (red) are the actual absorbance of mixed solution and the fitted spectra (blue) for the absorbance of a two-type single reactive species are superposed.

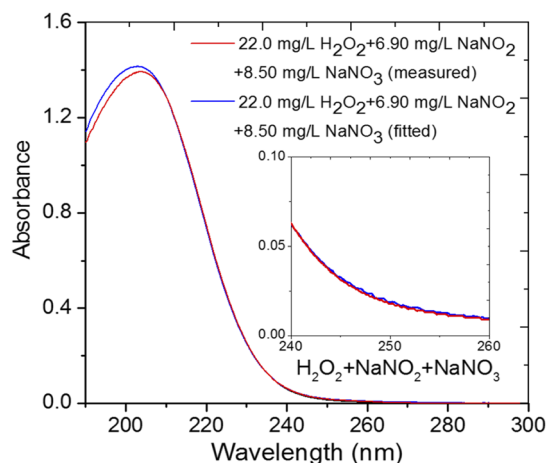


FIG. 4. Absorption spectrum of $\text{H}_2\text{O}_2+\text{NaNO}_2+\text{NaNO}_3$ mixed solution. The measured spectrum is the actual absorbance of a mixed solution and the fitted spectrum for the absorbance of two-type single reactive species is superposed.

a spectrophotometer instead of by using chemical probes. The fundamental goal of this work is to resolve this problem. Based on the results shown in Figs. 1–4, we conclude that only H_2O_2 contributes to the absorption spectrum above 250 nm, so the main solution is that the H_2O_2 absorbance is separated from total absorbance, with the remaining absorbance being due to NO_2^- and NO_3^- . Based on the results shown in Fig. 1(a), the fitting functions are obtained from the relationship between the known H_2O_2 concentration and absorbance at 250, 252.5, and 255 nm, respectively. These fitting functions are shown in Fig. 5. All fitting functions are almost linear at 250, 252.5, and 255 nm, respectively, and are given as follows:

$$A_{250} = \varepsilon_{250}(\text{H}_2\text{O}_2)l = 7.247 \times 10^{-4} \times n(\text{H}_2\text{O}_2) \quad \text{at 250 nm}, \quad (2)$$

$$A_{252.5} = \varepsilon_{252.5}(\text{H}_2\text{O}_2)l = 6.214 \times 10^{-4} \times n(\text{H}_2\text{O}_2) \quad \text{at 252.5 nm}, \quad (3)$$

$$A_{255} = \varepsilon_{255}(\text{H}_2\text{O}_2)l = 5.315 \times 10^{-4} \times n(\text{H}_2\text{O}_2) \quad \text{at 255 nm}, \quad (4)$$

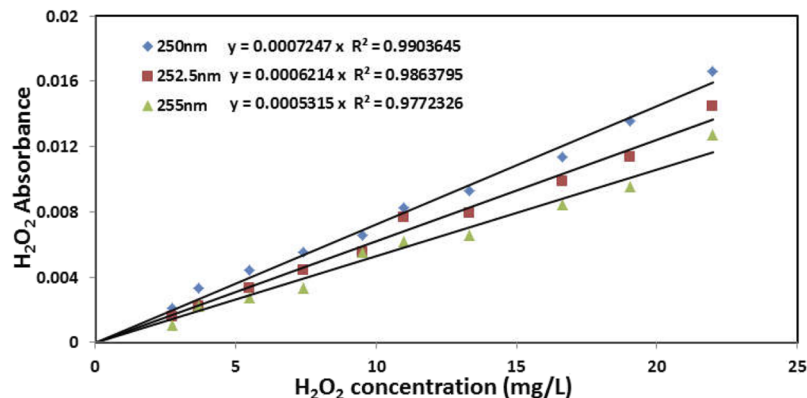


FIG. 5. H_2O_2 absorbance versus H_2O_2 concentration at 250, 252.5, and 255 nm.

where $n(\text{H}_2\text{O}_2)$ denotes the concentration of H_2O_2 in solution, A_{250} , $A_{252.5}$, and A_{255} are the absorbances at 250, 252.5, and 255 nm, respectively, and $l = 1$ cm is the optical path length. Given the absorbance from mixed solutions or from PAW at 250, 252.5, and 255 nm, we obtain the quantitative concentration of H_2O_2 by choosing an appropriate wavelength. Thus, the formula for calculating the H_2O_2 concentration is

$$n(\text{H}_2\text{O}_2) = [A_{250}/7.247 \times 10^{-4}] \text{ or } [A_{252.5}/6.214 \times 10^{-4}] \text{ or } [A_{255}/5.315 \times 10^{-4}] \quad (5)$$

D. Absolute concentrations of NO_3^- and NO_2^- in PAW

Based on the conclusions from Figs. 2–4, when the pH of a solution changes in Fig. 2 or when many species are mixed together in solution, as in Figs. 3 and 4, the actual measured absorption spectra and the fitted absorption spectra show a certain discrepancy between 200 and 220 nm. This result may be due to the pH affecting the absorbance between 200 and 220 nm because the ionization of NO_2^- and H_2O_2 significantly influences the absorbance with increasing H^+ concentrations. The influence of hybrid species is due to physical and chemical reactions, such as the oxidation of H_2O_2 , and to intermolecular forces.

However, in the tail of the absorption spectra (beyond 220 nm) for NO_2^- and NO_3^- , the UV absorption spectra are basically the same in Figs. 2–4, so the reasons above motivate us to choose any wavelength greater than 220 nm to fit the relationship between concentration and absorbance. A unique advantage of this approach is that the pH and hybrid species do not affect the absorbance because of the similarity of the tails of the absorption spectra, which effectively eliminates any error and does not affect the result for the concentration of NO_2^- and NO_3^- .

The concentrations of NO_3^- and NO_2^- are obtained based on the known concentration of H_2O_2 obtained by using Eq. (5). At a certain wavelength, the total absorbance of the solution is a superposition of absorptivity multiplied by the concentration. The resulting formula is

$$A_\lambda = \alpha n(\text{NO}_3^-) + \beta n(\text{NO}_2^-) + \varepsilon n(\text{H}_2\text{O}_2). \quad (6)$$

To more quickly and intuitively obtain the concentration of each RONS, we introduce a matrix to facilitate the calculation by an automated curve-fitting program. The absorbance at a given wavelength is defined as the product between the matrix of coefficients and a vector of concentrations:

$$\begin{pmatrix} A_{\lambda_1} \\ A_{\lambda_2} \end{pmatrix} / l = \begin{pmatrix} \alpha(\lambda_1) & \beta(\lambda_1) & \varepsilon(\lambda_1) \\ \alpha(\lambda_2) & \beta(\lambda_2) & \varepsilon(\lambda_2) \end{pmatrix} \begin{pmatrix} n(\text{NO}_3^-) \\ n(\text{NO}_2^-) \\ n(\text{H}_2\text{O}_2) \end{pmatrix} \quad (7)$$

To determine the concentration of the substance, the matrix can be transformed as follows:

$$\begin{pmatrix} n(\text{NO}_3^-) \\ n(\text{NO}_2^-) \\ n(\text{H}_2\text{O}_2) \end{pmatrix} = \begin{pmatrix} \alpha(\lambda_1) & \beta(\lambda_1) & \varepsilon(\lambda_1) \\ \alpha(\lambda_2) & \beta(\lambda_2) & \varepsilon(\lambda_2) \end{pmatrix}^{-1} \begin{pmatrix} A_{\lambda_1} \\ A_{\lambda_2} \end{pmatrix} / l, \quad (8)$$

where α , β , and ε are the molar absorptivity coefficients and can be obtained by fitting the concentration and absorbance

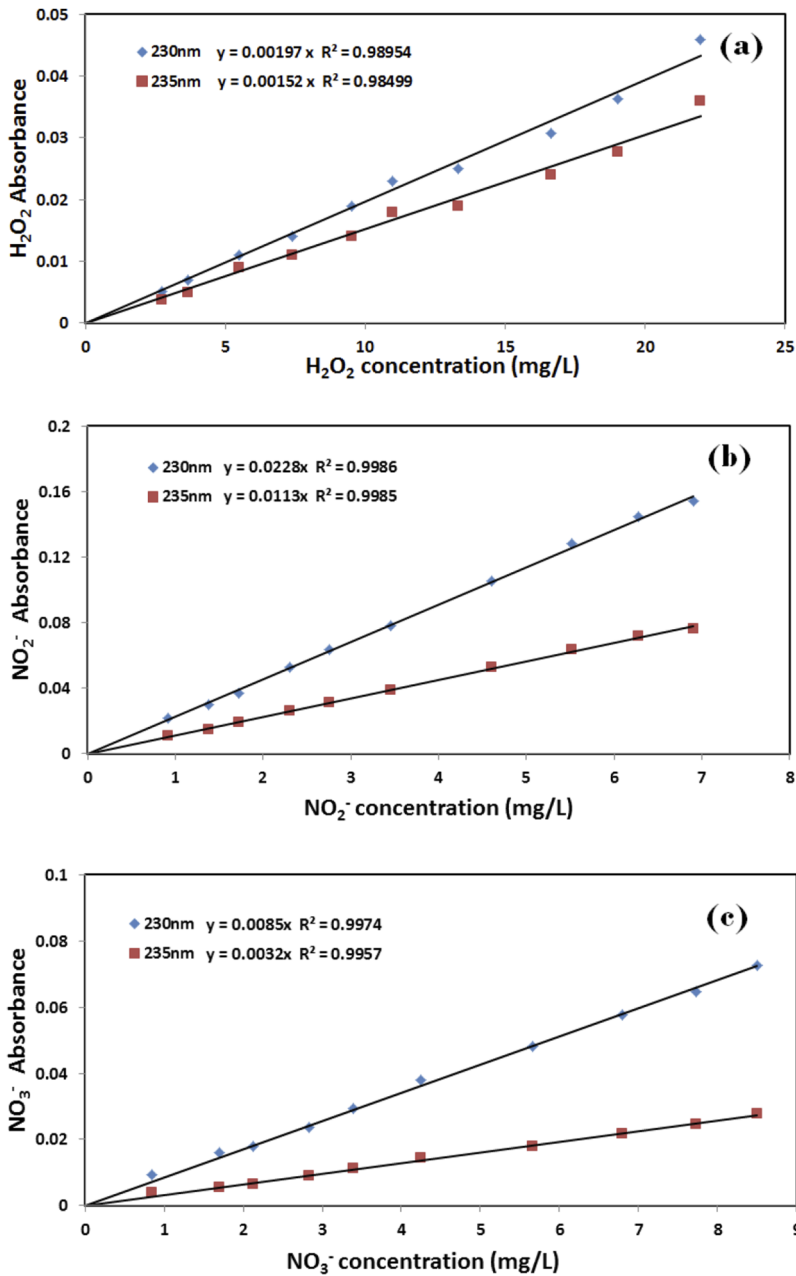


FIG. 6. Absorbance of (a) H₂O₂, (b) NO₂⁻, and (c) NO₃⁻ versus concentration at 230 and 235 nm.

functions of a single particle at a specified wavelength. A_λ in the vector is the absorption at wavelength λ .

Furthermore, to fit the relationship between concentration and absorbance and obtain the molar absorptivity coefficient, we select at random two absorption wavelengths (230 and 235 nm) within the wavelength range 220–250 nm. The relationships between concentration and absorbance for H_2O_2 , NO_2^- , and NO_3^- are shown in Figs. 6(a)–6(c), respectively. These results show that the absorbance of H_2O_2 , NO_2^- and NO_3^- is linear in concentration. Note that, at 230 and 235 nm, the PAW absorbance measured by UV-Vis spectrophotometer is the sum of three species: H_2O_2 , NO_2^- , and NO_3^- . Thus, according to Fig. 6, the two formulas for calculating the absorbance based on Eq. (8) are

$$0.0020 \times n(\text{H}_2\text{O}_2) + 0.0228 \times n(\text{NO}_2^-) + 0.0085 \times n(\text{NO}_3^-) \\ = A_{230} \quad \text{at 230nm,} \quad (9)$$

$$0.0015 \times n(\text{H}_2\text{O}_2) + 0.0113 \times n(\text{NO}_2^-) + 0.0032 \times n(\text{NO}_3^-) \\ = A_{235} \quad \text{at 235nm,} \quad (10)$$

where $n(\text{H}_2\text{O}_2)$, $n(\text{NO}_3^-)$, and $n(\text{NO}_2^-)$ are the concentrations of H_2O_2 , NO_3^- , and NO_2^- , respectively, in units of mg/L. The coefficients A_{230} and A_{235} are the absorbance at 230 and 235 nm, respectively. Putting the known values of $n(\text{H}_2\text{O}_2)$ from Eq. (5) into Eqs. (9) and (10) gives $n(\text{NO}_3^-)$ and $n(\text{NO}_2^-)$, respectively. Equations (5), (9), and (10) are thus proposed for determining the RONS concentration in PAW with the help of UV absorption spectroscopy. This approach allows the concentration of H_2O_2 , NO_2^- , and NO_3^- to be calculated given the total absorption spectra for PAW.

E. Verifying the accuracy of RONS concentrations

To verify the accuracy of the results obtained from Eqs. (5), (9), and (10), we compare the results of experiments wherein various plasma treatment times, applied voltages, and plasma-water distances are used. The goal is to calculate the concentration of H_2O_2 , NO_2^- , and NO_3^- in solution by using Eqs. (5), (9), and (10) and comparing the results with those obtained by using a microplate reader and adding chemical reagents. Figure 7 shows a flow chart

describing the experimental procedure, and a detailed presentation of the surface discharge generator used in the experiment is available in Ref. 31. The surface generator was used to produce a stable room-temperature surface air plasma, which was then used to treat deionized water in a petri dish under a given parametrization. A volume of 2 mL of the treated deionized water was put into a quartz cuvette to measure its absorption spectrum by using the UV-Vis spectrophotometer. All UV absorption spectra were recorded and processed by using a PC equipped with software that implemented the requisite formulas. A volume of 2 mL of treated deionized water was also distributed over 96-well plates to be measured by microplate reader with added chemical reagents.

Figure 8 shows the PAW UV absorbance for various plasma-treatment times, applied voltages, and plasma-water distances. The absorption spectrum is quite similar to that for the $\text{H}_2\text{O}_2 + \text{NaNO}_2 + \text{NaNO}_3$ mixed solutions (see Fig. 4), which confirms that the reactive species H_2O_2 , NO_3^- , and NO_2^- are the main long-lived chemical constituents in PAW. In addition, the absorbances grow almost linearly with increasing plasma-treatment time, applied voltage, and plasma-water distance, which indicates that the generation and diffusion rates of the reactive species produced by the surface-discharge plasma are very stable for transporting into water. Furthermore, the absorption spectra are similar but not identical. Upon closer inspection, the central peaks blueshift slightly upon increasing the plasma exposure, applied voltage, or plasma-water distance. These differences in peak profiles reveal a change in the RONS concentration and in the ratio of the RONS dose in PAW.

Figure 9 compares the calculated results and the results measured by using the microplate reader and shows that the two results are fairly consistent. The discrepancies between the measured and calculated results are attributed to several causes. The first cause is the error coefficient when fitting the curve, which is due to the limited accuracy of the spectrophotometer. Second, the pH and cross reactivity when mixing multiple species affects the fits, and this effect cannot be completely eliminated. Third, the microplate reader measures a product produced by a series of chemical reactions with a reagent, and incomplete chemical reactions also lead

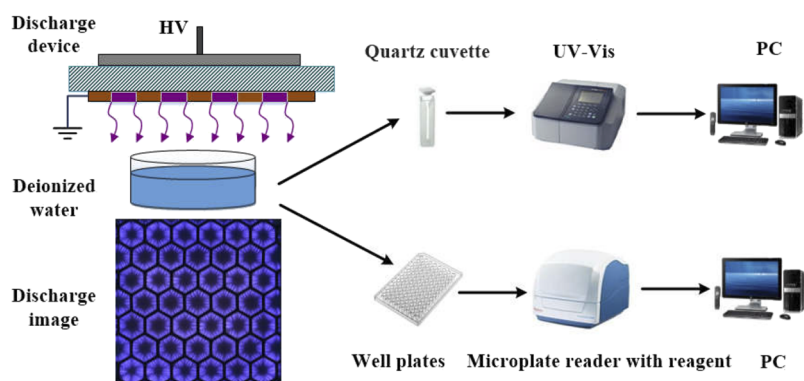


FIG. 7. Experimental apparatus for surface discharge generator and a detailed flow chart of the experimental procedure for measuring RONS concentration.

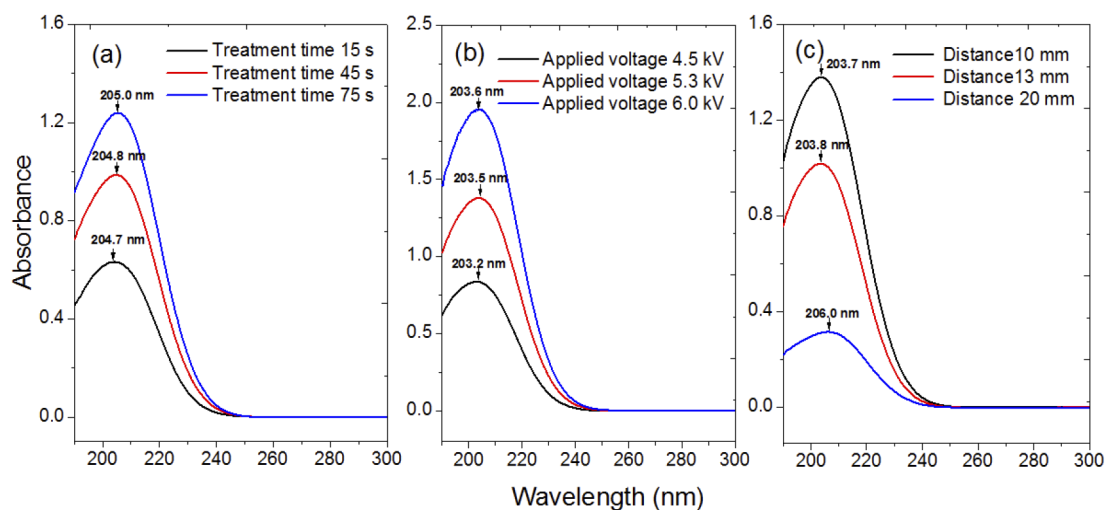


FIG. 8. PAW absorbance versus wavelength for various plasma treatment times, applied voltages, and plasma-water distances. (a) Applied voltage is 5.3 kV and plasma-water distance is 10 mm. (b) Plasma-treatment time is 45 s and plasma-water distance is 10 mm. (c) Applied voltage is 5.3 kV and plasma-treatment time is 45 s.

to errors. Fourth, the ambient temperature and humidity also affect the absorption spectra and the characteristics of the surface-discharge plasma.

However, the errors caused by these four factors fall within an acceptable range. The accuracy of the results for the concentration of H_2O_2 , NO_3^- , and NO_2^- is reasonable compared with the known concentrations of the standard solutions. Thus, the formulas used to fit the UV absorption are suitable for calculating the concentration of H_2O_2 , NO_3^- , and NO_2^- in PAW. In addition, the dose of RONS delivered into solution is easy to control quantitatively by adjusting the plasma exposure time, applied voltage, and plasma-water distances.

F. Time- and depth-resolved RONS concentrations

Because the time-dependent concentration of RONS in PAW is quite significant for biomedical applications, we measured the temporally and spatially resolved concentration of RONS. We measured the real-time, depth-resolved UV absorption spectra (Ocean Optics, USB 2000+) to analyze the liquid phase and investigate temporal variations during direct plasma treatment of deionized water. Because the UV-Vis spectrophotometer used in the work described above allowed us to determine and fix the measurement point through a quartz cuvette, we used this instrument instead of the UV-Vis spectrophotometer for making real-time measurements.

Figure 10(a) shows a schematic diagram of a measurement system that used a surface-discharge plasma to directly treat deionized water in a quartz cuvette. Details of the measurement and recording process can be found in our previous report.³¹ Figures 10(b) and 10(c) show the PAW absorption spectra as measured by UV-Vis and UV absorption spectroscopy and for various plasma-treatment times

and applied voltages. The absorption spectra are exactly the same above 225 nm, which indicates that Eqs. (5), (9), and (10) may be used with these spectra to calculate the concentration of H_2O_2 , NO_3^- , and NO_2^- in PAW. This is another reason we choose the wavelengths greater than 220 nm to fit the spectra. The difference in the PAW absorption spectra below 220 nm in Figs. 10(b) and 10(c) is attributed to the inability of the UV absorption spectrometer to measure absorbance at these short wavelengths, and the accuracy of the absorption spectrum near 200 nm is degraded by absorbance in the cuvette.

The experimental setup depicted in Fig. 10 allowed us to monitor the RONS concentration in real-time and at different depths. The total absorbance is positively correlated with the total concentration of RONS, and the total absorbance spectrum reflects the total concentration of RONS, so we measured the total absorbance to determine the total concentrations of RONS. The total absorbance (range: 200–300 nm) is plotted in Fig. 11 as a function of plasma-treatment time and for different depths (5, 10, 15, and 20 mm) along the vertical axis. The total absorbance is defined as²⁸

$$\begin{aligned} \text{Total absorbance} &\approx \int_{200\text{nm}}^{300\text{nm}} \text{ABS}(\lambda) d\lambda \\ &\approx \text{Total RONS concentration.} \end{aligned} \quad (11)$$

Figure 11 shows that a delay time of approximately 90 s precedes the appearance of RONS in PAW at a depth of 5 mm whereas essentially no RONS exists at 20 mm depth, which indicates that this delay time may depend on the penetration depth. At greater depths, a lower total absorbance, which corresponds to a smaller concentration of RONS, can be detected in the PAW. For the measurement of RONS at a depth of 5 mm, after the ~90 s delay time, the upstream RONS reaches the measurement point at 5 mm by diffusion, so the total

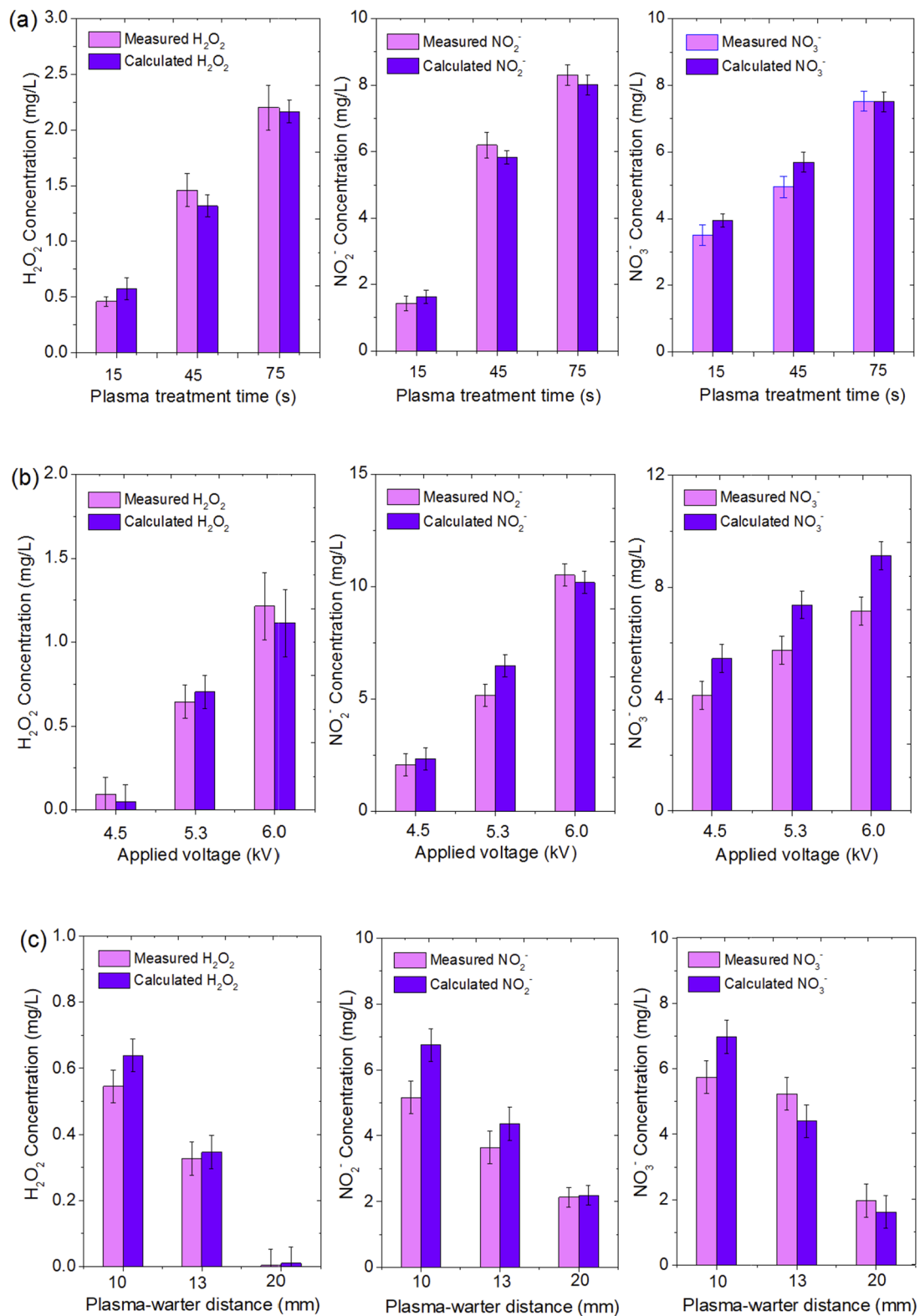


FIG. 9. Calculated concentrations of H₂O₂, NO₃⁻, and NO₂⁻ and concentrations measured by using the microplate reader for various (a) plasma-treatment times, (b) applied voltages, and (c) plasma-water distances.

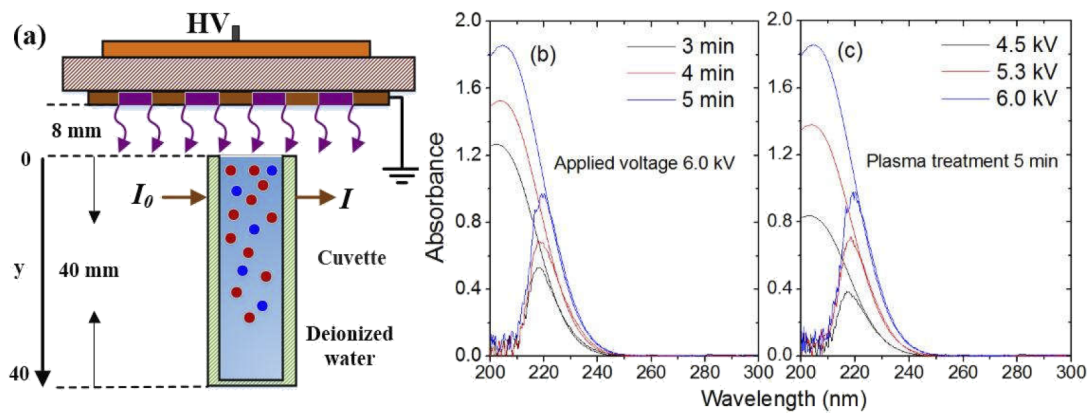


FIG. 10. (a) Schematic diagram of measurement system. PAW absorbance was measured by UV-Vis and UV absorption spectroscopy at different (b) treatment times and (c) applied voltages.

absorbance gradually increases with treatment time. When the plasma is turned off after 5 min. so that the RONS are no longer generated, the total absorbance continues to rise due to the RONS accumulated upstream of the 5 mm measurement point. At about 6 min, the total absorbance at 5 mm begins to decrease, which indicates a reduced RONS concentration at 5 mm and a continued downward diffusion of RONS in PAW. The same phenomenon is also detected at the other measurement depths. However, no downward diffusion of RONS occurs at 15 mm, so the concentration approaches zero at 20 mm. Finally, note that the delay time depends on the penetration depth and the rate at which RONS is produced by the plasma source.

Next, we use Eqs. (5), (9), and (10) to calculate the absorption spectra at 5, 10, and 15 mm (the RONS concentration at 20 mm is too small to analyze) and obtain the RONS

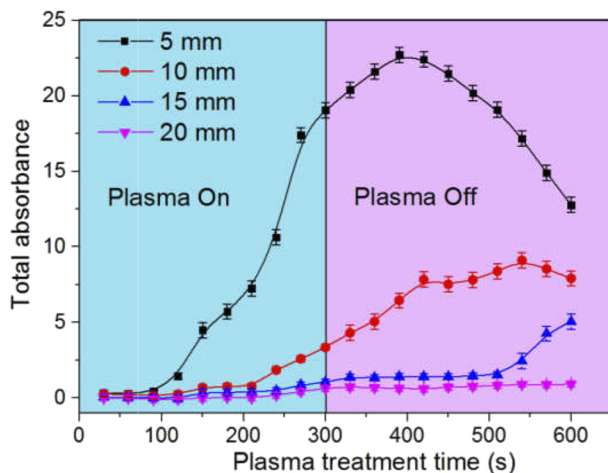


FIG. 11. Total absorbance in PAW as a function of plasma-treatment time. In all cases, the treatment time was 5 min (blue zone), after which the plasma was turned off (pink zone).

concentration as a function of plasma-treatment time at the different depths (see Fig. 12). The concentrations of H_2O_2 , NO_3^- , and NO_2^- follow dynamics similar to that of the total absorbance shown in Fig. 11. At 5 mm, after approximately 100 s delay, the concentration of NO_2^- and NO_3^- begins to increase rapidly and, after 220 s, the concentration of H_2O_2

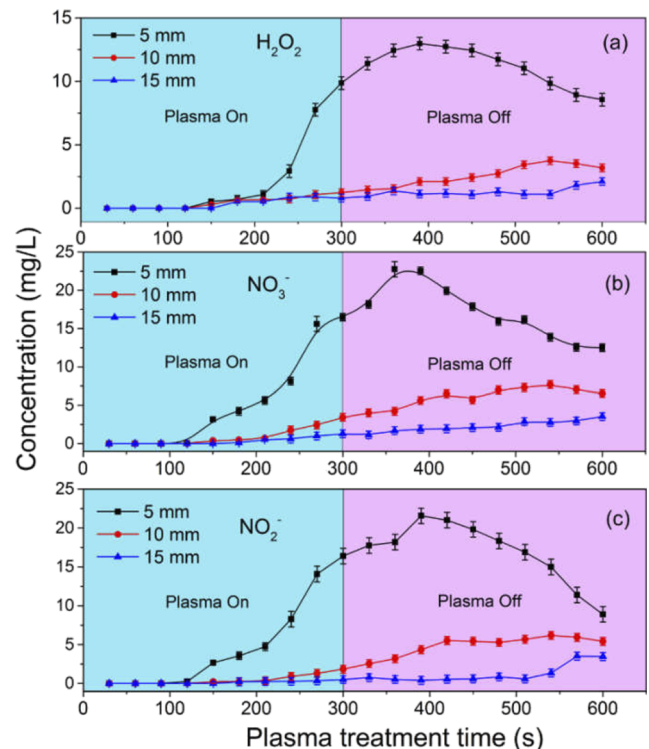


FIG. 12. Concentration as a function of plasma-treatment time of (a) H_2O_2 , (b) NO_3^- , and (c) NO_2^- in PAW [calculated by using Eqs. (5), (9), and (10)]. The treatment time in all cases was 15 min (blue zone), after which the plasma was turned off (pink zone).

begins to increase rapidly. At 100 s after the plasma is turned off, the concentration of RONS begins to decrease, the generation rate of H_2O_2 becomes the slowest, and the generation rate of NO_2^- drops the fastest. At 10 and 15 mm, the concentration of RONS also increases gradually due to diffusion of the upstream RONS.

The time-dependent concentration of RONS in PAW is very important for biomedical applications. For example, to eradicate cells in tumors, the RONS needs to be generated throughout the tissue fluid so that they can penetrate cell membranes and react with intracellular components.^{41,42} Thus, the diffusion process of RONS and the spatial and temporal distribution of RONS concentration at different times and depths must be understood in detail. In addition, the RONS dose must be controlled at the target depth so that the RONS can eliminate germs without affecting normal tissues.⁴³ This method to monitor and control the concentration of H_2O_2 , NO_3^- , and NO_2^- should aid the development of new models for predicting and analyzing plasma interactions with water and provide an in-depth commentary of implications that other is still exploring. We expect that the proposed method will provide new insights into the concentration and the penetration depth of H_2O_2 , NO_3^- , and NO_2^- in water. Although this method is presently suitable only for measurements in PAW, it facilitates the measurement of long-lived reactive species. Further research should allow bio-related liquids other than deionized water to be used, such as normal saline, phosphate buffered saline, etc., which would have a big impact on plasma biomedical applications.

IV. CONCLUSIONS

This paper proposes an optics-based method to accurately measure the concentration of long-lived reactive species (H_2O_2 , NO_3^- , and NO_2^-) in PAW without adding any chemical reagents and provides the corresponding formulas for calculating these concentrations. This approach constitutes a simple and useful way to determine the concentration of RONS by overcoming the problem of experimental error caused by the different pH values that occur upon mixing H_2O_2 , NO_3^- , and NO_2^- . To confirm the veracity of the calculated concentrations, we also measured the concentration of H_2O_2 , NO_2^- , and NO_3^- by using a microplate reader and adding chemical reagents under different parametrizations. In addition, we measured the spatial distribution and the penetration of RONS in PAW, which we analyzed in real time by using UV absorption spectroscopy. When the plasma is turned on, the concentration of RONS gradually increases with treatment time and, when the plasma is turned off, the concentration of RONS continues to rise for a certain time and then begins to decrease. This measurement method may provide new insights into the spatial and temporal distribution of RONS in PAW.

ACKNOWLEDGMENTS

This work was supported by the National Natural Science Foundation of China (Grant Nos. 51707150, 51677147, and

51521065), the China Postdoctoral Science Foundation (Grant No. 2017M613134 and 2017M610639), the Shaanxi Province Postdoctoral Science Foundation (2017BSHYDZZ11), and the State Key Laboratory of Electrical Insulation and Power Equipment (Grant No. EIPE 17309).

REFERENCES

- ¹D. B. Graves, *Plasma Process. Polym.* **11**, 1120 (2014).
- ²P. Lukes, E. Dolezalova, I. Sisrovaand, and M. Clupek, *Plasma Sources Sci. Technol.* **23**, 015019 (2014).
- ³M. G. Kong, G. Kroesen, G. Morfill, T. Nosenko, T. Shimizu, J. Van Dijk, and J. L. Zimmermann, *New J. Phys.* **11**, 115012 (2009).
- ⁴M. J. Traylor, M. J. Pavlovich, S. Karim, P. Hait, Y. Sakiyama, D. Clark, and D. B. Graves, *J. Phys. D: Appl. Phys.* **44**, 472001 (2011).
- ⁵D. B. Graves, *Phys. Plasmas* **21**, 080901 (2014).
- ⁶K. D. Weltmann and T. V. Woedtke, *Plasma Phys. Control. Fusion* **59**, 014031 (2014).
- ⁷Z. J. Liu, D. H. Xu, D. X. Liu, Q. J. Cui, H. F. Cai, Q. S. Li, H. L. Chen, and M. G. Kong, *J. Phys. D: Appl. Phys.* **50**, 195204 (2017).
- ⁸D. X. Liu, Z. C. Liu, C. Chen, A. J. Yang, D. Li, M. Z. Rong, H. L. Chen, and M. G. Kong, *Sci Rep.* **6**, 23737 (2016).
- ⁹W. Tian, A. M. Lietzand, and M. J. Kushner, *Plasma Sources Sci. Technol.* **25**, 055020 (2015).
- ¹⁰K. Oehmigen, M. Hahnel, R. Brandenburg, C. Wilke, K. D. Weltmann, and T. V. Woedtke, *Plasma Process. Polym.* **7**, 250 (2010).
- ¹¹N. Kurake, H. Tanaka, K. Ishikawa, K. Takeda, H. Hasizume, K. Nakamura, H. Kajiyama, T. Kondo, F. Kikkawa, M. Mizune, and M. Hori, *J. Phys. D: Appl. Phys.* **50**, 155202 (2017).
- ¹²P. M. Girard, A. Arbabian, M. Fleury, G. Bauville, V. Puech, M. Dutreix, and J. S. Sousa, *Sci Rep.* **6**, 29098 (2016).
- ¹³D. B. Graves, *J. Phys. D: Appl. Phys.* **45**, 263001 (2012).
- ¹⁴H. Tresp, M. U. Hammer, K. D. Weltmann, and S. Reuter, *Plasma Med.* **3**, 45 (2013).
- ¹⁵H. Tresp, M. U. Hammer, K. D. Weltmann, and S. Reuter, *J. Phys. D: Appl. Phys.* **46**, 435401 (2013).
- ¹⁶W. Tian and M. J. Kushner, *J. Phys. D: Appl. Phys.* **47**, 165201 (2014).
- ¹⁷Z. J. Liu, D. X. Liu, D. H. Xu, H. F. Cai, W. J. Xia, B. C. Wang, Q. S. Li, and M. G. Kong, *J. Phys. D: Appl. Phys.* **50**, 195203 (2017).
- ¹⁸X. Lu, G. V. Naidis, M. Laroussi, and K. Ostrikov, *Phys. Rep.* **540**, 123 (2014).
- ¹⁹N. Kumar, J. H. Park, S. N. Jeon, B. S. Park, E. H. Choi, and P. Attri, *J. Phys. D: Appl. Phys.* **49**, 115401 (2016).
- ²⁰S. J. Kim and T. H. Chung, *Sci Rep.* **6**, 20332 (2016).
- ²¹H. Y. Wu, P. Sun, H. Feng, H. X. Zhou, R. X. Wang, Y. D. Liang, J. F. Lu, W. D. Zhu, J. Zhang, and J. Fang, *Plasma Process. Polym.* **9**, 417 (2012).
- ²²K. C. Hsieh, R. J. Wandell, S. Bresch, and B. R. Locke, *Plasma Process. Polym.* e1600171 (2017).
- ²³E. J. Baek, H. M. Joh, S. J. Kim, and T. H. Chung, *Phys. Plasmas* **23**, 073515 (2016).
- ²⁴J. S. Oh, E. J. Szili, K. Ogawa, R. D. Short, M. Ito, H. Furuta, and A. Hatta, *Jpn. J. Appl. Phys.* **57**, 0102B9 (2018).
- ²⁵S. Dikalov, M. Skatchkov, and E. Bassenge, *Biochem. Bioph. Res. Commun.* **230**, 54 (1997).
- ²⁶H. Xu, C. Chen, D. X. Liu, D. H. Xu, Z. J. Liu, X. H. Wang, and M. G. Kong, *J. Phys. D: Appl. Phys.* **50**, 245201 (2017).
- ²⁷J. S. Oh, E. J. Szili, N. Gaur, S. H. Hong, H. Furuta, H. Kurita, A. Mizuno, A. Hatta, and R. D. Short, *J. Phys. D: Appl. Phys.* **49**, 304005 (2016).
- ²⁸E. J. Szili, J. S. Oh, and S. H. Hong, *J. Phys. D: Appl. Phys.* **48**, 202001 (2015).
- ²⁹J. S. Oh, M. Kakuta, H. Furuta, H. Akatsuka, and A. Hatta, *Jpn. J. Appl. Phys.* **55**, 06HD01 (2016).
- ³⁰S. Baldus, D. Schroder, N. Bibinov, V. Schulz-von der Gathen, and P. Awakowicz, *J. Phys. D: Appl. Phys.* **48**, 275203 (2015).

- ³¹T. T. He, D. X. Liu, H. Xu, Z. J. Liu, D. H. Xu, D. Li, Q. S. Li, M. Z. Rong, and M. G. Kong, *J. Phys. D: Appl. Phys.* **49**, 205204 (2016).
- ³²P. Lu, D. Boehm, P. Bourke, and P. J. Cullen, *Plasma Process. Polym.* **14**, 1600207 (2017).
- ³³B. B. He, Y. P. X. Ma, X. N. Gong, Z. J. Long, J. S. Li, Q. Xiong, H. Liu, Q. Chen, X. H. Zhang, S. Z. Yang, and Q. H. Liu, *J. Phys. D: Appl. Phys.* **50**, 445207 (2017).
- ³⁴Z. Machala, B. Tarabova, K. Hensel, E. Spetlikova, L. Sikurovaand, and P. Lukes, *Plasma Processes Polym.* **10**, 649 (2013).
- ³⁵H. Jablonowski, M. C. Hansch, M. Dunnbier, K. Wende, M. U. Hammer, K. D. Weltman, S. Reuter, and T. Woedtke, *Biointerphases*. **10**, 029506 (2015).
- ³⁶Z. T. Chen, L. Lin, X. Q. Cheng, E. Gjika, and M. Keidar, *Plasma Process. Polym.* **13**, 1151 (2016).
- ³⁷K. P. Arjunan, A. Obrusnik, B. T. Jones, L. Zajickova, and S. Ptasinska, *Plasma Process. Polym.* **13**, 1089 (2016).
- ³⁸M. J. Traylor, M. J. Pavlovich, S. Karim, P. Hait, Y. Sakiyama, D. S. Clark, and D. B. Graves, *J. Phys. D: Appl. Phys.* **44**, 472001 (2011).
- ³⁹S. Ikawa, K. Kitano, and S. Hamaguchi, *Plasma Process. Polym.* **7**, 33 (2010).
- ⁴⁰D. Yan, J. H. Sherman, X. Cheng, E. Ratovitski, J. Canady, and M. Keidar, *Appl. Phys. Lett.* **105**, 224101 (2014).
- ⁴¹M. Keidar, R. Walk, A. Shashurin, P. Srinivasan, A. Sandler, S. Dasgupta, R. Ravi, R. Guerrero-Preston, and B. Trink, *Br. J. Cance.* **105**, 1295 (2011).
- ⁴²K. Oehmigen, J. Winter, M. Hähnel, C. Wilke, R. Brandenburg, K. D. Weltmann, and T. von Woedtke, *Plasma Process. Polym.* **8**, 904 (2013).
- ⁴³S. H. Hong, E. J. Szili, A. T. A. Jenkins, and R. D. Short, *J. Phys. D: Appl. Phys.* **47**, 362001 (2014).